THE JOURNAL OF PHYSICAL CHEMISTRY C
A JOURNAL OF THE AMERICAN CHEMICAL SOCIETY
pubs.acs.org/JPCC Article

# Superconductivity in Nonstoichiometric Rubidium-Doped $C_{60}$

Li-Na Zong, Ren-Shu Wang, Di Peng, and Xiao-Jia Chen*



Cite This: J. Phys. Chem. C 2022, 126, 2912−2919 Read Online



**ABSTRACT:** A wet-chemical method is used to synthesize rubidium-doped $C_{60}$ samples. Superconductivity with a critical temperature of 22−23 K is identified from the magnetization and resistivity measurements based on the Meissner effect and the zero-resistivity state. Raman scattering measurements show a downshift of $16 \pm 1$ cm$^{-1}$ for the $A_g(2)$ vibrational mode, yielding a charge transfer of less than 3, which puts the new superconductor in the face-centered cubic structure based on the well-established phase diagram for this system. The superconducting parameters, such as the critical current density, the lower and upper critical field, and the derived coherence length and penetration depth, are determined from multiple techniques for this superconductor.

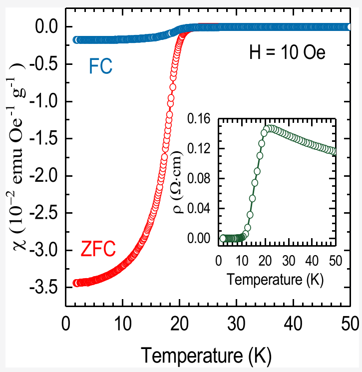




## ■ INTRODUCTION

The discovery of the method for the synthesis of a large quantity of fullerene compounds[1] has greatly stimulated the chemical and physical studies on the interesting material, $C_{60}$, especially for the alkali-metal-doped $C_{60}$ with superconductivity. The first fullerene superconductor was discovered in K-doped $C_{60}$ with a critical temperature ($T_c$) of 18 K.[2] Since then, alkali-metal-doped fullerites with higher $T_c$s were reported consecutively, and the highest $T_c$ of 33 K was soon achieved in the ternary compound, $Cs_2RbC_{60}$, at ambient pressure.[3] In the next decade, the improvement of $T_c$ for alkali-metal-doped fullerites has come to a standstill. In this period, most works focusing on improved synthesis methods,[4−9] and the characterization of all kinds of superconducting parameters for the known materials has been reported continually, especially for $K_3C_{60}$ and $Rb_3C_{60}$. The record of the highest $T_c$ was not broken until superconductivity was achieved in $Cs_3C_{60}$ under pressure with the record high $T_c$ of 38 K for this family.[10] The discovery of superconductivity in Cs-doped $C_{60}$ has also ignited great interest in the discussion of the pairing mechanisms of superconductivity for this compound[11−14] due to its abnormal antiferromagnetic insulating parent state and the dome-like evolution of $T_c$ under high pressure. Therefore, the importance of the electron correlation effect has attracted more attention since then apart from the electron−phonon coupling effect.

In alkali-metal-doped fullerene superconductors, Rb-doped $C_{60}$ is the second reported superconductor with a much higher $T_c$ of 28 K[15] compared with $K_3C_{60}$. And the binary compounds are easily handled compared with ternary and even quaternary compounds due to the difficulties on the precise control of stoichiometry. Based on the conventional BCS theory, the increased $T_c$ upon the substitution of alkali atoms with larger radii was attributed to the increasing density of states at the Fermi level. Therefore, a linear correlation between the $T_c$s and the lattice constants of the doped $C_{60}$ molecules was established.[16] Though numerous works have been done on $Rb_3C_{60}$, including structure,[16−19] Raman spectroscopy,[20−23] and magnetization studies[4−6,9,15,24−29] as well as electrical and electronic property measurements[30−36] and many other characterizations and analysis, the consensus on the determination of all kinds of superconducting parameters has not been reached. The measured parameters vary widely from laboratory to laboratory, from measuring method by method, even from sample by sample prepared by the same group. The wide variation of these parameters is likely due to poorly prepared samples with heterogeneous compositions. For most Rb-doped $C_{60}$ superconductors, the evidence for superconductivity was often obtained either through the Meissner effect from the magnetization measurements or by the zero-resistance state from the resistivity measurements. It is highly desired to detect both the Meissner effect and zero-resistance state from the same sample as the unequivocal evidence to support superconductivity. In previous studies, the superconductivity was usually reported in samples with a doping level of exactly 3.[4,18,37,38] In fact, the phase diagram of Rb-doped $C_{60}$ with

**Received:** December 9, 2021
**Revised:** January 12, 2022
**Published:** January 31, 2022

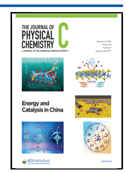




https://doi.org/10.1021/acs.jpcc.1c10420
J. Phys. Chem. C 2022, 126, 2912−2919

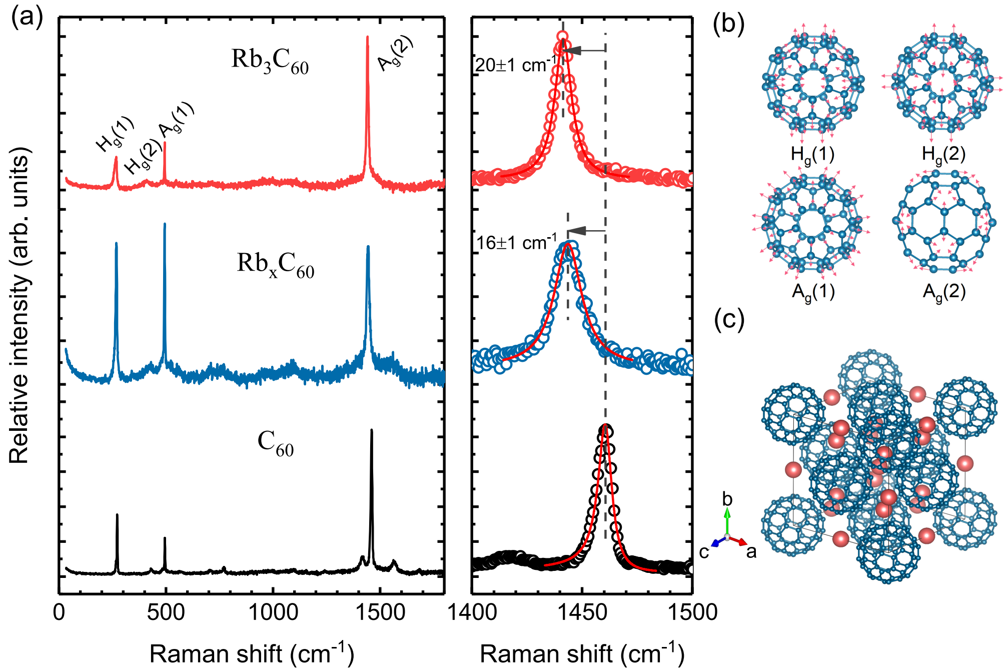


**Figure 1.** Raman spectra of pristine and Rb-doped $C_{60}$ compounds at room temperature. (a) Left panel: Raman spectra for pristine $C_{60}$, $Rb_xC_{60}$, and $Rb_3C_{60}$ as labeled above the curves. The background of the Raman spectra is subtracted for clarity. The vibrational modes for Rb-doped $C_{60}$ are marked on the curve for $Rb_3C_{60}$. Right panel: An expanded view of the $A_g(2)$ modes for the specified samples on the left panel (the hollow circles) and the Lorentz fitting curves (red solid lines). The downshift of the $A_g(2)$ modes upon doping is marked on the curves. (b) Mode vibrations for $H_g(1)$, $H_g(2)$, $A_g(1)$, and $A_g(2)$ modes, respectively. (c) Schematic crystal structure based on the established phase diagram and crystal structure.[17] The red balls represent rubidium atoms.

doping is quite rich, in which the face-centered cubic structure persists up to a large stoichiometry.[17] The reported resistivity results for underdoped $Rb_xC_{60}$ in the stoichiometric range of 2−3 were very close to those for $Rb_3C_{60}$.[39] Besides, the Fermi energy cutoff like that for metallic $Rb_3C_{60}$ has also been observed in underdoped $Rb_xC_{60}$.[40] In early studies on the connections between charge carriers and $T_c$, a rapid drop of $T_c$ was reported in fullerides when the valence deviates from 3.[41] The depressed $T_c$ was also reported in a recent work for K-doped $C_{60}$ with a nonstoichiometric doping level deviating from 3.[42] It is interesting to examine whether superconductivity can take place with a low valence close to 2 and whether a noninteger dopant matters for superconductivity.

The key to solving these issues is to synthesize homogeneous and high-quality fulleride superconductors. For such a purpose, we adopt a modified solution-phase doping method to synthesize a Rb-doped $C_{60}$ sample. Both magnetization and resistivity measurements are applied to identify the superconductivity in the same sample, which are further used to estimate the superconducting parameters. All results are obtained from the same well-characterized sample to ensure the repeatability and accuracy of experimental data for the comparison with existing models and for future theoretical model developments and identifications.

## ■ MATERIALS AND METHODS

Rb-doped $C_{60}$ samples were synthesized by a wet-chemical method as well-described in a previous work.[43] The pristine fullerene was purchased from Tokyo Chemical Industry with a purity larger than 99.5% and used without further purification. The alkali-metal rubidium (99.75%) was purchased from Alfa Aesar. Rigorously dried tetrahydrofuran solvent was applied in our reaction to eliminate the negative impact of the side reactions. Based on the acquired synthesis method, we made some modifications to accelerate the reaction and to acquire a more homogeneous sample. Sonication treatment under mild heating for about 9 min was performed before the mechanical mixing process. To get a better-crystallized sample with a higher shielding fraction, the annealing treatment was conducted at 200 °C for 48 h with a heating rate of 2−3 °C per minute followed by a natural cooling process in an inert gas atmosphere. The prepared Rb-doped samples were then sealed in capsules and glass capillary tubes for the magnetization and Raman scattering measurements, respectively. All the manipulation mentioned above was performed in a glovebox with both $O_2$ and $H_2O$ contents of less than 0.01 ppm. The electrical transport results were obtained from the same sample that has been well-characterized by magnetization measurements.

Raman spectroscopy was conducted in an in-house system with a charge coupled device and spectrometer from Princeton Instruments. The air-sensitive Rb-doped $C_{60}$ samples were sealed in fused glass capillary tubes before characterization. An excitation wavelength of 488 nm and a laser power less than 1 mW were adopted to avoid the possible radiation damage of pristine $C_{60}$, and the same excitation wavelength and a laser power less than 2 mW were applied for Rb-doped samples. The integration time was kept at 2 min. The magnetization $M(T)$ of the Rb-doped $C_{60}$ samples sealed in the nonmagnetic capsules was measured in a SQUID magnetometer (Quantum Design) with given magnetic fields. The Physical Property Measurement System (Quantum Design) was applied for the electrical resistivity measurements. The electrical resistivity ($\rho$) was measured using a DC four-probe Van Der Pauw configuration. The specially designed Be−Cu cell equipped


https://doi.org/10.1021/acs.jpcc.1c10420
J. Phys. Chem. C 2022, 126, 2912−2919

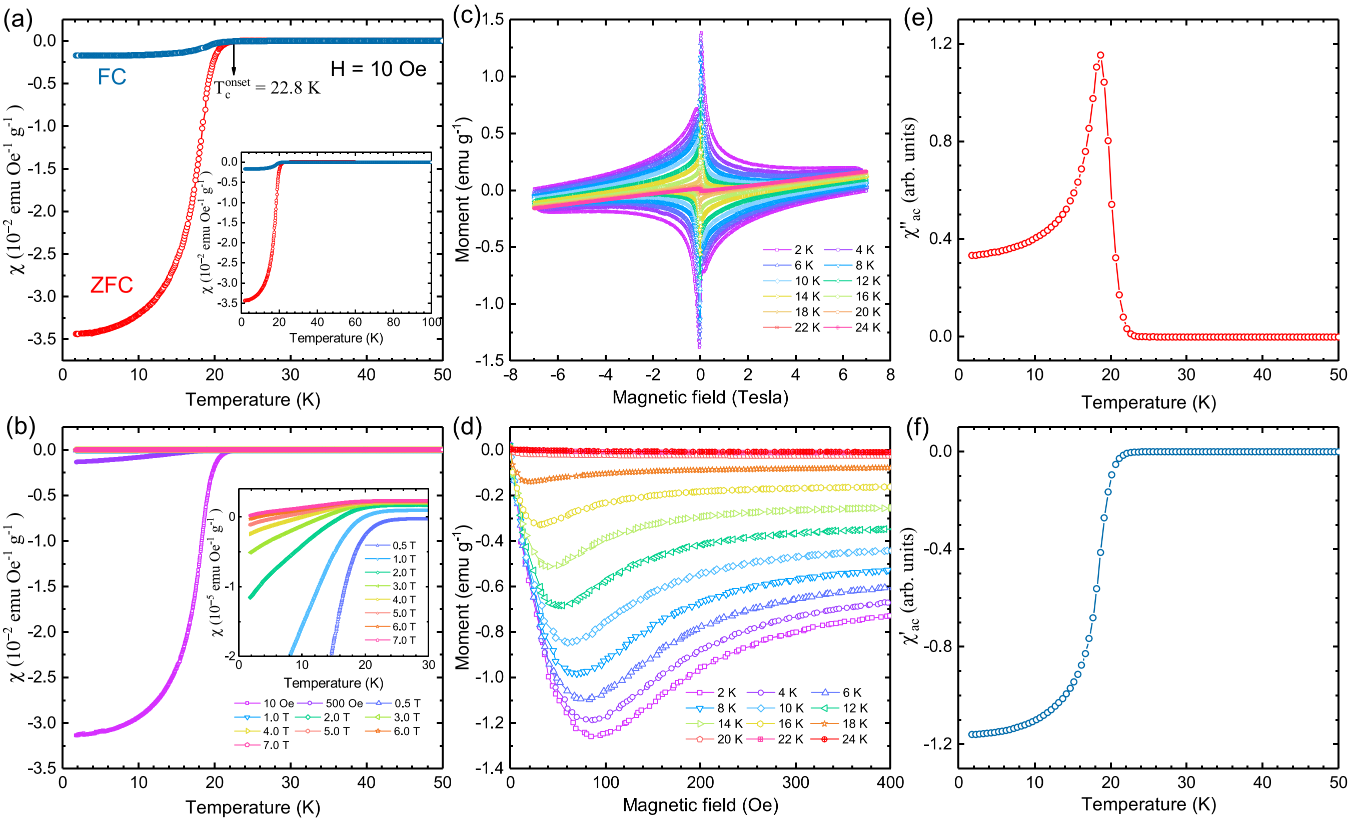


**Figure 2.** Magnetization characterization for Rb-doped $C_{60}$. (a) Temperature dependence of the zero-field-cooled (ZFC) and field-cooled (FC) magnetic susceptibility with an applied field of 10 Oe at the temperature range of 1.8−50 K. Inset: A full view of the susceptibility curves in the range of 1.8−100 K. (b) Temperature-dependent ZFC magnetic susceptibility at various applied magnetic fields. Inset: An expanded view for the susceptibility curves with magnetic fields ranging from 0.5 to 7 T. (c) Magnetic hysteresis loops with a magnetic field up to ±7 T at indicated temperatures. (d) Low magnetic-field dependence of the magnetization up to 400 Oe at temperature intervals of 2 K up to 24 K. (e) Temperature-dependent imaginary ($\chi''$) part of the *ac* susceptibility. (f) Real ($\chi'$) part of the *ac* susceptibility. The probe magnetic amplitude and frequency are set as 5 Oe and 234 Hz, respectively.

with four airtight copper leads was adopted to protect the highly air-sensitive samples.

## ■ RESULTS AND DISCUSSION

Raman spectroscopy measurements were performed to get the knowledge of the vibrational modes and charge transfer for the synthesized $C_{60}$ samples. Figure 1(a) shows the room-temperature Raman spectra of pristine $C_{60}$ and Rb-doped $C_{60}$. Upon doping, the overall intensity of the Raman spectra for the Rb-doped samples decrease to about one-third of that for pristine $C_{60}$ (not shown). This phenomenon has been reported in previous work,[23] which can be attributed to the decreased penetration depth of the laser in alkali-metal-doped $C_{60}$ with a narrower band gap or even with a metallic state. For the parent compound with a face-centered cubic structure, active Raman modes include two $A_g$ and eight $H_g$ modes. Upon doping, only the lowest two $H_g$ modes and two $A_g$ modes remain observable on the curves for our Rb-doped $C_{60}$ samples, which is reminiscent of the previous works.[20] The mode vibrations for the dominant modes upon doping are depicted in Figure 1(b), two $H_g$ modes being part of low-energy radial motions and two $A_g$ modes belonging to high-energy tangential motions. Besides, the $H_g(1)$ mode for Rb-doped $C_{60}$ exhibits a Breit−Wigner−Fano line shape, and this character is consistent with that reported for $K_3C_{60}$ and $Rb_3C_{60}$ films,[21,44] further illustrating that the collected data are derived from the doped products. Based on previous exploration, the downshift of the $A_g(2)$ mode upon alkali-metal doping is generally recognized as a measure for the charge transfer.[20,45] The empirical linear correlation is one electron transfer corresponds to a redshift of 6−7 $cm^{-1}$ for this $A_g$ mode.[23,45] This linear correlation has been established both for K-doped and Rb-doped $C_{60}$.[46,47] With different doping levels, the Rb-doped $C_{60}$ compounds have different crystal structures and exhibit different Raman active modes as depicted for K-doped $C_{60}$.[23,48] In previous works, for $RbC_{60}$, the downshift of the $A_g(2)$ mode is about 6 $cm^{-1}$, much less than our synthesized sample; the downshift of about 30 $cm^{-1}$ for the $A_g(2)$ mode is attributed to $Rb_6C_{60}$, and the downshift of about 20 $cm^{-1}$ belongs to $Rb_3C_{60}$.[47] Therefore, the Raman shift for $Rb_4C_{60}$ is in the range of 20−30 $cm^{-1}$ following the linear correlation. Besides, for $RbC_{60}$, the face-centered cubic structure exhibiting the similar Raman active modes as our synthesized samples generally exists at high temperature, and the room-temperature phase is an orthorhombic structure with much more Raman active modes alongside the $A_g(2)$ mode.[46] In addition, for another stable phase $Rb_6C_{60}$ with a body-centered cubic structure, apart from the different downshift of the $A_g(2)$ mode, the number of the Raman active modes is even more than that for pristine $C_{60}$ as depicted in previous works.[20] For our synthesized sample, the $A_g(2)$ mode exhibits a single-band feature, and no traces belonging to $RbC_{60}$, $Rb_4C_{60}$, and $Rb_6C_{60}$ can be detected, indicating that our sample is a well-doped single-phase compound. As shown on the right panel of Figure


https://doi.org/10.1021/acs.jpcc.1c10420
J. Phys. Chem. C 2022, 126, 2912−2919

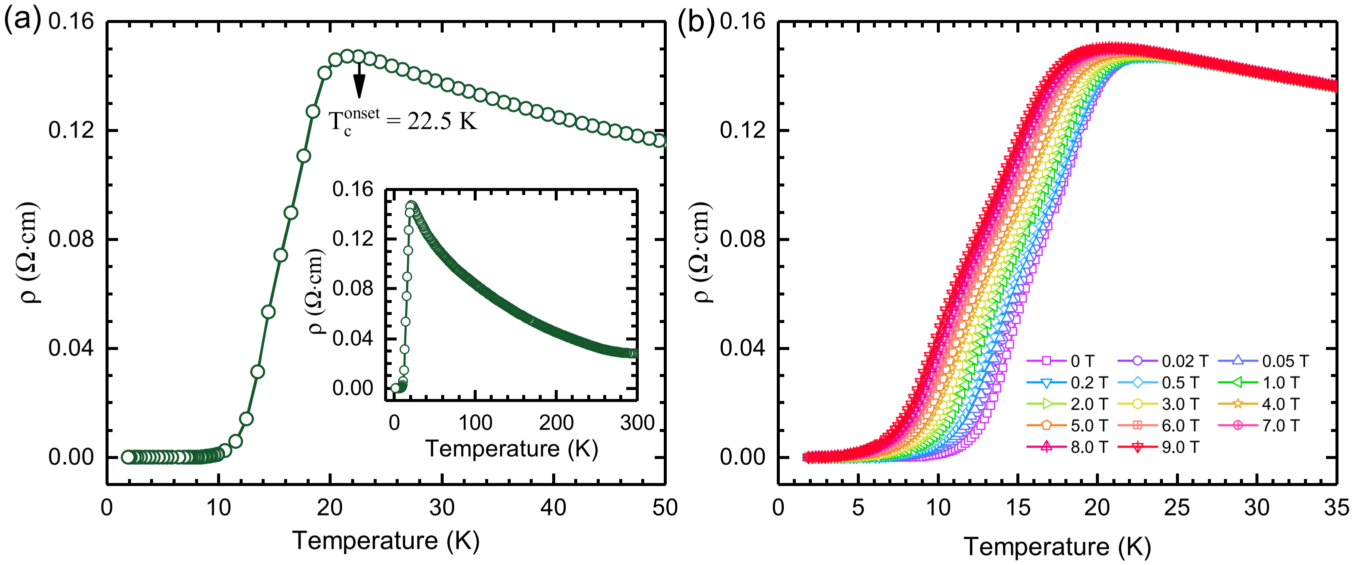


**Figure 3.** Temperature-dependent electrical resistivity ($\rho$) of Rb-doped $C_{60}$. (a) $\rho(T)$ in the temperature range of 2−50 K at zero magnetic field. The inset shows the resistivity curve in the full temperature range of 2−300 K. (b) $\rho(T)$ at various magnetic fields in the low-temperature range of 2−35 K.

1(a), the 16 ± 1 $cm^{-1}$ downshift of the $A_g(2)$ mode for $Rb_xC_{60}$ is slightly lower than that for $Rb_3C_{60}$ of about 20 $cm^{-1}$, indicating that the charge transfer in our sample is less than 3. We presume that the refined stoichiometry for our synthesized sample deviates from the integer 3, residing in a doping level of 2−3. The nonstoichiometric doped samples have been found both in K-doped and Rb-doped $C_{60}$ prepared by the vapor-transport method.[17,40,49] Most previous works concentrate on the studies of the vibrational and electronic properties for these materials, but few explore whether superconductivity can be realized in these nonstoichiometric doped samples. Based on the phase diagram for Rb-doped $C_{60}$ proposed by Zhu et al.,[17] our sample resides in the first two-phase coexisting range and possesses the face-centered cubic structure. As shown in Figure 1(c), we give a provisional crystal structure for $Rb_xC_{60}$ in terms of that for $Rb_3C_{60}$.[18] To explore further, magnetization measurements were carried out on the Rb-doped $C_{60}$ sample to explore whether superconductivity can be achieved in this sample.

The Meissner effect and zero-resistance state are two essential properties for a well-defined superconductor. Both *dc* and *ac* magnetic susceptibility measurements were performed to elucidate the Meissner effect of the Rb-doped $C_{60}$. Figure 2(a) shows the temperature dependence of the magnetic susceptibility for Rb-doped $C_{60}$. The sample was first cooled down to 1.8 K in zero field, and data were then taken in a given magnetic field of 10 Oe on warming the sample to 100 K, corresponding to a zero-field-cooling run (ZFC). Then, the sample was cooled in the same magnetic field to the lowest temperature to collect the field-cooling run (FC) data simultaneously. The ZFC magnetization shows the flux exclusion, while the FC magnetization displays the flux expulsion. The big difference between the two curves is evidence for trapped flux and often detected in type-II superconductors. The overall magnetization behavior demonstrates the well-defined Meissner state with an onset $T_c$ of 22.8 K. The $T_c$ is far different from that reported for $Rb_3C_{60}$ of about 28 K,[15] indicating that the nonstoichiometric Rb-doped $C_{60}$ sample may correspond to a new superconducting phase.

The depressed $T_c$ may originate from the lesser charge transfer upon nonstoichiometric Rb intercalation according to our Raman spectra. According to previous studies, $T_c$ is proportional to the density of states at the Fermi level, which can be affected by the lattice constant and carrier concentration.[16,41] Supposing that the density ($\delta$) for our sample is about 2 g $cm^{-3}$, the shielding fraction (SF) is estimated to be about 88% (SF = $4\pi\chi\delta$) at 1.8 K with an applied magnetic field of 10 Oe, which is a comparatively high value for powdered samples.[4,7,9] Figure 2(b) demonstrates the suppression of $T_c$ by the applied fields, which is a typical feature for superconductivity. The inset of Figure 2(b) gives an expanded view for the overlapped curves in high fields. Figure 2(c) represents the magnetization hysteresis loops with a magnetic field along two opposite directions up to 7 T at a temperature step of 2 K. The magnetization of our sample decreases with increasing temperature and completely converges at 24 K. The diamond-like shape of the hysteresis loops indicates that the Rb-doped sample is a typical type-II superconductor. Based on Bean's critical-state model,[50] one can get an estimation of the critical current density ($J_c$) from these hysteresis curves. Figure 2(d) depicts the variation of the magnetization with increasing magnetic field up to 400 Oe at various temperatures, obtained by using the same method just as the hysteresis loops, which is a common method to determine the lower critical field $[H_{c1}(T)]$ for superconductors. The temperature dependence of the *ac* susceptibility further confirms the superconductivity for our sample and can also be recognized as a qualitative criterion for the sample quality. The imaginary part ($\chi''$) shown in Figure 2(e) is correlated with the energy dissipation in the sample due to the formation of a superconducting vortex current.[51] The real part ($\chi'$) displayed in Figure 2(f) of the *ac* susceptibility is a measure of the magnetic shielding, in accordance with the ZFC run in *dc* magnetization measurement. Both the $\chi'$ and $\chi''$ parts exhibit an obvious anomaly at around 22 K, resembling the diamagnetic transition in *dc* measurements. Note that a narrow peak appears in the $\chi''$ part when the magnetic field penetrates to the centers of the sample grains during measurement. The single sharp peak appearing in


https://doi.org/10.1021/acs.jpcc.1c10420
J. Phys. Chem. C 2022, 126, 2912−2919

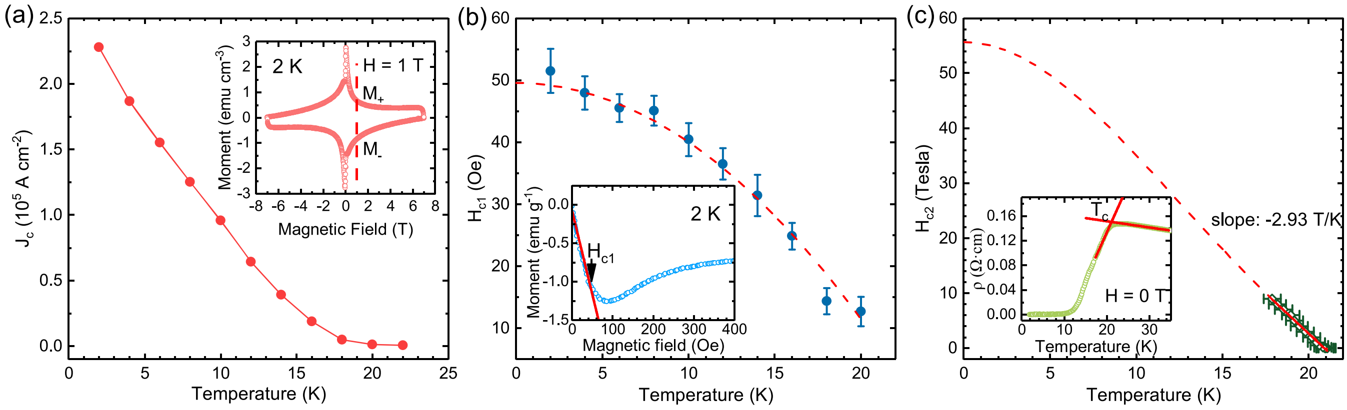


**Figure 4.** Characterization of superconducting parameters for Rb-doped $C_{60}$. (a) Temperature dependence of the critical current density at the given magnetic field. The solid line is a guide to the eye. The inset shows the method to determine the $M_+$ and $M_-$ with a specific magnetic field of 1 T at 2 K. (b) Temperature-dependent lower critical field $H_{c1}(T)$ determined by $M(H)$ at low magnetic fields. The dashed line represents the nonlinear fitting based on the empirical law $H_{c1}(T)/H_{c1}(0) = 1 - (T/T_c)^2$. Inset: $H_{c1}(T)$ is defined as the field where a deviation from a linear $M(H)$ occurs. Error bars represent the estimated uncertainties in determining $H_{c1}(T)$. (c) Determination of the upper critical field $H_{c2}(T)$. The dashed line depicts the nonlinear fit based on the Ginzburg–Landau theory, and the solid line represents the linear fit of the $dH_{c2}(T)/dT$. The error bars reflect the rounding of the transition. The inset illustrates the method of determining $T_c$ from the resistivity curve at an applied field of 0 T.

$\chi''$ part demonstrates that the Rb-doped $C_{60}$ sample possesses one superconducting phase and exhibits bulk superconducting features. Since the well-characterized $\chi''$ part can be a qualitative criterion for samples with zero resistivity, the electrical resistivity measurements are performed to study the electrical properties of our sample.

The electrical resistivity measurements were performed on the same sample that has been characterized by magnetization measurements. Before the measurements, the powdered sample was pressed into a compact pellet to reduce the poor contact. Figure 3(a) shows the $\rho(T)$ of the Rb-doped $C_{60}$ sample at a low-temperature range of 2–50 K at zero field and demonstrates that zero resistivity has been achieved in our sample. The inset of Figure 3(a) depicts the full view of the resistivity curve in a temperature range up to 300 K. The critical temperature is defined as the highest point on the resistivity curve, which agrees fairly well with that determined by magnetic measurements. Below 22.5 K, the resistivity starts to decrease; zero resistivity is obtained at about 10 K. The transition width for the sample, defined as the temperature range from 10 to 90% of the transition, is 6.4 K and is comparable to that reported for powdered samples.[2] Besides, the normal-state resistivity increases by a factor of 4 with decreasing temperature in the studied temperature range, which can be attributed to the granular effect as reported for $K_3C_{60}$ films.[52] The nonmetallic normal-state resistivity can also be attributed to the nonsuperconducting part in our sample, because the shielding fraction is not 100% and defects or sample inhomogeneity may exist. Figure 3(b) displays the variation of $\rho(T)$ under different external magnetic fields. Upon increasing magnetic field, the broadened transition width and the depressed $T_c$ can be observed evidently, which are the intrinsic properties for superconductivity and are reminiscent of those reported for $Rb_3C_{60}$.[32] The suppression of $T_c$ by the applied magnetic fields can also be adopted to evaluate the upper critical field [$H_{c2}(T)$] for our sample.

Therefore, both Meissner effect and zero-resistance state are realized as solid evidence for superconductivity in our nonstoichiometric Rb-doped $C_{60}$ sample. Our work also makes up the lack on the determination of the superconductivity for one sample from the both intrinsic properties in Rb-doped $C_{60}$.

Based on the available data from the measurements of the magnetic and electrical transport properties, we determined the superconducting parameters for the Rb-doped $C_{60}$ sample. Figure 4(a) shows the temperature dependence of the $J_c$ at the given magnetic field of 1 T. For a cylindrical sample with radius $R$ (cm), the $J_c(H,T)$ can be calculated using the formula:[53] $J_c(H) = 15 \times (M_+ - M_-)/R$, where $M_+$ and $M_-$ represent the magnetization at the indicated external field measured by increasing and decreasing magnetic field at a specified temperature. The inset of Figure 4(a) depicts the method to determine the $M_+$ and $M_-$ on the hysteresis loop at 2 K. Assuming the grain size of our sample is 1 $\mu$m, we obtain $J_c(T = 2\text{ K}, H = 1\text{ T}) = 2.25 \times 10^5$ A cm$^{-2}$, which is lower by an order of magnitude than that for $Rb_3C_{60}$ at the same magnetic field at low temperatures.[24,25] As shown in Figure 4(a), the $J_c$ of our sample decreases with increasing temperature, which is in accord with the previous works for $K_3C_{60}$ and $Rb_3C_{60}$.[54]

Figure 4(b) shows the temperature-dependent $H_{c1}$ for the Rb-doped $C_{60}$ sample. The inset of Figure 4(b) depicts the method to determine the $H_{c1}$ at 2 K, which is defined as the field where the deviation from a linear $M(H)$ occurs. The $H_{c1}(0)$ of our sample is estimated to be about 49.6 ± 2.6 Oe, which is obtained by the nonlinear fit based on the empirical law $H_{c1}(T)/H_{c1}(0) = 1 - (T/T_c)^2$. This value just resides in the wide range of $H_{c1}(0)$ for $Rb_3C_{60}$ with a maximum of about 16 mT and a minimum of about 0.9 mT.[25,29] Apart from this method, the trapped magnetic moment method is also adopted to determine $H_{c1}(T)$ for alkali-metal-doped fulleride superconductors but usually gives a lower value.[55]

Figure 4(c) depicts the determination of $H_{c2}(T)$ for our sample. The $H_{c2}(T)$ is weighed by the method as exhibited in the inset of Figure 4(c). Namely, the intersection of the linear extrapolations made both below and above $T_c$ defines $H_{c2}(T)$. Based on the Werthamer-Helfand-Hohenberg equation,[56] $H_{c2}(0) = 0.693[-(dH_{c2}/dT)]_{Tc}T_c$, the slope is fitted to be −2.93 T/K and the calculated $H_{c2}(0)$ is about 42.8 ± 0.8 T. $H_{c2}(0)$ is about 55.6 ± 1.4 T by fitting $H_{c2}(T)$ with the expression $H_{c2}(T) = H_{c2}(0)[1 - (T/T_c)^2]/[1 + (T/T_c)^2]$


https://doi.org/10.1021/acs.jpcc.1c10420
J. Phys. Chem. C 2022, 126, 2912−2919

based on the Ginzburg–Landau theory. In previous studies of $H_{c2}(0)$ for $Rb_3C_{60}$, many techniques have been applied to acquire a reliable value, including magnetization,[25,57,58] electrical transport,[32] and radio frequency.[59,60] All these methods give variable results ranging from 78 to 38 T depending on samples and measuring techniques. Taking the range of $T_c$ into consideration, the extrapolated $H_{c2}(0)$ for our sample is in a reasonable range for alkali-metal-doped $C_{60}$ superconductors.

Using the relations[61] $H_{c2}(0) = \Phi_0/2\pi\xi^2$ and $H_{c1}(0) = (\phi_0/4\pi\lambda_L^2)\ln(\lambda_L^2/\xi)$, where $\Phi_0$ is flux quantum, the zero-temperature coherence length $\xi$ and the penetration depth $\lambda_L$ for our sample are estimated to be 2.4 and 408.5 nm, respectively. The penetration depth is in the intermediate range of that for $Rb_3C_{60}$ and very close to a result of 420 nm obtained by the muon spin relaxation method.[25,32,62] The coherence length of our sample is comparable to those reported for $Rb_3C_{60}$ measured by electrical transport and radio frequency methods.[32,59] The Ginzburg–Landau parameter $\kappa = \lambda/\xi$ of about 170 is obtained, which further confirms the type-II superconductor character.

## ■ CONCLUSIONS

In conclusion, we have synthesized a high-quality Rb-doped $C_{60}$ sample using a wet-chemical method. Upon doping, the charge transfer is determined by the downshift of $16 \pm 1$ cm$^{-1}$ for the $A_g(2)$ mode, yielding a charge transfer of less than 3, which indicates that the synthesized sample is a non-stoichiometric doped compound. Based on the established knowledge, we give a provisional crystal structure and the specific mode vibrations for our synthesized sample. Moreover, both the Meissner effect and zero-resistivity state with $T_c$ in the range of 22–23 K have been detected to provide solid evidence of superconductivity for our sample. The lesser charge transfer consistent with the different $T_c$ values and bulk superconductivity characters may demonstrate that we have synthesized a new superconducting phase and also prove superconductivity can be realized in samples with a valence state deviating from exactly 3 for Rb-doped $C_{60}$. Furthermore, the superconducting parameters, including $J_c(T = 2\text{ K}, H = 1\text{ T}) = 2.25 \times 10^5$ A cm$^{-2}$, $H_{c1}(0) = 49.6 \pm 2.6$ Oe, $H_{c2}(0) = 55.6 \pm 1.4$ T, and the derived $\xi = 2.4$ nm and $\lambda_L = 408.5$ nm, are well-defined by multiple techniques. Our work provides both magnetic and electrical transport evidence for one sample with superconductivity, making the determination of superconducting parameters more canonical and reliable. Furthermore, the correlation of the carrier concentration with $T_c$ needs further experimental and theoretical exploration, which may contribute to understanding what controls superconductivity in fullerene superconductors.

## ■ AUTHOR INFORMATION

### Corresponding Author

**Xiao-Jia Chen** − *Center for High Pressure Science and Technology Advanced Research, Shanghai 201203, China; School of Science, Harbin Institute of Technology, Shenzhen 518055, China;* orcid.org/0000-0003-3921-9424; Phone: +86 (0)21 80177044; Email: xjchen@hpstar.ac.cn; Fax: +86 (0)21 80177 064

### Authors

**Li-Na Zong** − *Center for High Pressure Science and Technology Advanced Research, Shanghai 201203, China;* orcid.org/0000-0003-0355-7229

**Ren-Shu Wang** − *School of Science, Harbin Institute of Technology, Shenzhen 518055, China; Center for High Pressure Science and Technology Advanced Research, Shanghai 201203, China*

**Di Peng** − *Center for High Pressure Science and Technology Advanced Research, Shanghai 201203, China;* orcid.org/0000-0002-4235-6385

Complete contact information is available at:
https://pubs.acs.org/10.1021/acs.jpcc.1c10420

### Notes

The authors declare no competing financial interest.

## ■ ACKNOWLEDGMENTS

This work was funded through the National Key R&D Program of China (Grant No. 2018YFA0305900), the Shenzhen Science and Technology Program (Grant No. KQTD20200820113045O8), and the Basic Research Program of Shenzhen (Grant No. JCYJ20200109112810241).

## ■ REFERENCES

(1) Kroto, H. W.; Heath, J. R.; O'Brien, S. C.; Curl, R. F.; Smalley, R. E. $C_{60}$: Buckminsterfullerene. *Nature* **1985**, *318*, 162–163.

(2) Hebard, A. F.; Rosseinsky, M. J.; Haddon, R. C.; Murphy, D. W.; Glarum, S. H.; Palstra, T. T. M.; Ramirez, A. P.; Kortan, A. R. Superconductivity at 18 K in potassium-doped $C_{60}$. *Nature* **1991**, *350*, 600–601.

(3) Tanigaki, K.; Ebbesen, T. W.; Saito, S.; Mizuki, J.; Tsai, J. S.; Kubo, Y.; Kuroshima, S. Superconductivity at 33 K in $Cs_xRb_yC_{60}$. *Nature* **1991**, *352*, 222–223.

(4) McCauley, J. P.; Zhu, Q.; Coustel, N.; Zhou, O.; Vaughan, G.; Idziak, S. H. J.; Fischer, J. E.; Tozer, S. W.; Groski, D. M. Synthesis, structure, and superconducting properties of single-Phase $Rb_3C_{60}$. A new, convenient method for the preparation of $M_3C_{60}$ superconductors. *J. Am. Chem. Soc.* **1991**, *113*, 8537–8538.

(5) Wang, H. H.; Kini, A. M.; Savall, B. M.; Carlson, K. D.; Williams, J. M.; Lathrop, M. W.; Lykke, K. R.; Parker, D. H.; Wurz, P. Superconductivity at 28.6 K in a rubidium-$C_{60}$ fullerene compound, $Rb_xC_{60}$, synthesized by a solution-phase technique. *Inorg. Chem.* **1991**, *30*, 2962–2963.

(6) Buffinger, D. R.; Ziebarth, R. P.; Stenger, V. A.; Recchia, C.; Pennington, C. H. Rapid and efficient synthesis of alkali metal-$C_{60}$ compounds in liquid ammonia. *J. Am. Chem. Soc.* **1993**, *115*, 9267–9270.

(7) Schlueter, J. A.; Wang, H. H.; Lathrop, M. W.; Geiser, U.; Carlson, K. D.; Dudek, J. D.; Yaconi, G. A.; Williams, J. M. ESR study of the formation of superconducting $Rb_3C_{60}$ from solution. *Chem. Mater.* **1993**, *5*, 720–725.

(8) Liu, X.; Wan, W. C.; Owens, S. M.; Broderick, W. E. Superconducting alkali metal fullerides: Development of a versatile solution-phase route from soluble $M_3C_{60}$ precursors. *J. Am. Chem. Soc.* **1994**, *116*, 5489–5490.

(9) Cooke, S.; Glenis, S.; Chen, X.; Lin, C. L.; Labes, M. M. New preparation of superconducting alkali-metal fullerides utilizing monomethylamine as solvent. *J. Mater. Chem.* **1996**, *6*, 1–3.

(10) Ganin, A. Y.; Takabayashi, Y.; Khimyak, Y. Z.; Margadonna, S.; Tamai, A.; Rosseinsky, M. J.; Prassides, K. Bulk superconductivity at 38 K in a molecular system. *Nat. Mater.* **2008**, *7*, 367–371.

(11) Takabayashi, Y.; Ganin, A. Y.; Jeglič, P.; Arčon, D.; Takano, T.; Iwasa, Y.; Ohishi, Y.; Takata, M.; Takeshita, N.; Prassides, K.; et al. The disorder-free non-BCS superconductor $Cs_3C_{60}$ emerges from an

antiferromagnetic insulator parent state. *Science* **2009**, *323*, 1585−1590.
(12) Ganin, A. Y.; Takabayashi, Y.; Jeglič, P.; Arčon, D.; Potočnik, A.; Baker, P. J.; Ohishi, Y.; McDonald, M. T.; Tzirakis, M. D.; McLennan, A.; et al. Polymorphism control of superconductivity and magnetism in $Cs_3C_{60}$ close to the Mott transition. *Nature* **2010**, *466*, 221−225.
(13) Zadik, R. H.; Takabayashi, Y.; Klupp, G.; Colman, R. H.; Ganin, A. Y.; Potočnik, A.; Jeglič, P.; Arčon, D.; Matus, P.; Kamarás, K.; et al. Optimized unconventional superconductivity in a molecular Jahn-Teller metal. *Sci. Adv.* **2015**, *1*, 1500059.
(14) Nomura, Y.; Sakai, S.; Capone, M.; Arita, R. Unified understanding of superconductivity and Mott transition in alkali-doped fullerides from first principles. *Sci. Adv.* **2015**, *1*, 1500568.
(15) Rosseinsky, M. J.; Ramirez, A. P.; Glarum, S. H.; Murphy, D. W.; Haddon, R. C.; Hebard, A. F.; Palstra, T. T. M.; Kortan, A. R.; Zahurak, S. M.; Makhija, A. V. Superconductivity at 28 K in $Rb_xC_{60}$. *Phys. Rev. Lett.* **1991**, *66*, 2830−2832.
(16) Fleming, R. M.; Ramirez, A. P.; Rosseinsky, M. J.; Murphy, D. W.; Haddon, R. C.; Zahurak, S. M.; Makhija, A. V. Relation of structure and superconducting transition temperatures in $A_3C_{60}$. *Nature* **1991**, *352*, 787−788.
(17) Zhu, Q.; Zhou, O.; Coustel, N.; Vaughan, G. B. M.; McCauley, J. P.; Romanow, W. J.; Fischer, J. E.; Smith, A. B., III X-ray diffraction evidence for nonstoichiometric rubidium-$C_{60}$ intercalation compounds. *Science* **1991**, *254*, 545−548.
(18) Fischer, J. E.; Bendele, G.; Dinnebier, R.; Stephens, P. W.; Lin, C. L.; Bykovetz, N.; Zhu, Q. Structural analysis of fullerene and fulleride solids from synchrotron x-ray powder diffraction. *J. Phys. Chem. Solids* **1995**, *56*, 1445−1457.
(19) Stephens, P. W.; Mihaly, L.; Wiley, J. B.; Huang, S.-M.; Kaner, R. B.; Diederich, F.; Whetten, R. L.; Holczer, K. Structure of Rb:$C_{60}$ compounds. *Phys. Rev. B* **1992**, *45*, 543−546.
(20) Duclos, S. J.; Haddon, R. C.; Glarum, S.; Hebard, A. F. Raman studies of alkali-metal doped $A_xC_{60}$ films (A = Na, K, Rb,and Cs; $x$ = 0, 3, and 6). *Science* **1991**, *254*, 1625−1627.
(21) Zhou, P.; Wang, K.-A.; Eklund, P. C.; Dresselhaus, G.; Dresselhaus, M. S. Raman-scattering study of the electron-phonon interaction in $M_3C_{60}$ (M = K,Rb). *Phys. Rev. B* **1993**, *48*, 8412−8417.
(22) Mitch, M. G.; Chase, S. J.; Lannin, J. S. Raman scattering and electron-phonon coupling in $Rb_xC_{60}$. *Phys. Rev. Lett.* **1992**, *68*, 883−886.
(23) Kuzmany, H.; Matus, M.; Burger, B.; Winter, J. Raman scattering in $C_{60}$ fullerenes and fullerides. *Adv. Mater.* **1994**, *6*, 731−745.
(24) Politis, C.; Buntar, V.; Krauss, W.; Gurevich, A. Magnetic properties of superconducting $Rb_3C_{60}$. *Europhys. Lett.* **1992**, *17*, 175−179.
(25) Sparn, G.; Thompson, J. D.; Whetten, R. L.; Huang, S.-M.; Kaner, R. B.; Diederich, F.; Grüner, G.; Holczer, K. Pressure and field dependence of superconductivity in $Rb_3C_{60}$. *Phys. Rev. Lett.* **1992**, *68*, 1228−1231.
(26) Ramirez, A. P.; Kortan, A. R.; Rosseinsky, M. J.; Duclos, S. J.; Mujsce, A. M.; Haddon, R. C.; Murphy, D. W.; Makhija, A. V.; Zahurak, S. M.; Lyons, K. B. Isotope effect in superconducting $Rb_3C_{60}$. *Phys. Rev. Lett.* **1992**, *68*, 1058−1060.
(27) Chen, C.-C.; Lieber, C. M. Isotope effect and superconductivity in metal-doped $C_{60}$. *Science* **1993**, *259*, 655−658.
(28) Diederichs, J.; Gangopadhyay, A. K.; Schilling, J. S. Pressure dependence of the electronic density of states and $T_c$ in superconducting $Rb_3C_{60}$. *Phys. Rev. B* **1996**, *54*, R9662−R9665.
(29) Buntar, V.; Sauerzopf, F. M.; Weber, H. W.; Halushka, M.; Kuzmany, H. Mixed state parameters of single crystalline $Rb_3C_{60}$ fullerene superconductors. *Phys. Rev. B* **2005**, *72*, 024521.
(30) Xiang, X.-D.; Hou, J. G.; Crespi, V. H.; Zettl, A.; Cohen, M. L. Three-dimentional fluctuation conductivity in superconducting single crystal $K_3C_{60}$ and $Rb_3C_{60}$. *Nature* **1993**, *361*, 54−56.
(31) Hebard, A. F.; Palstra, T. T. M.; Haddon, R. C.; Fleming, R. M. Absence of saturation in the normal-state resistivity of thin films of $K_3C_{60}$ and $Rb_3C_{60}$. *Phys. Rev. B* **1993**, *48*, 9945−9948.
(32) Hou, J. G.; Xiang, X.-D.; Crespi, V. H.; Cohen, M. L.; Zettl, A. Magnetotransport in single-crystal $Rb_3C_{60}$. *Physica C* **1994**, *228*, 175−180.
(33) Burk, B.; Crespi, V. H.; Zettl, A.; Cohen, M. L. Rubidium isotope effect in superconducting $Rb_3C_{60}$. *Phys. Rev. Lett.* **1994**, *72*, 3706−3709.
(34) Koller, D.; Martin, M. C.; Mihály, L.; Mihály, G.; Oszlányi, G.; Baumgartner, G.; Forró, L. Energy gap in superconducting fullerides: Optical and tunneling studies. *Phys. Rev. Lett.* **1996**, *77*, 4082−4085.
(35) Fuhrer, M. S.; Cherrey, K.; Zettl, A.; Cohen, M. L.; Crespi, V. H. Carbon isotope effect in single-crystal $Rb_3C_{60}$. *Phys. Rev. Lett.* **1999**, *83*, 404−407.
(36) Hesper, R.; Tjeng, L. H.; Heeres, A.; Sawatzky, G. A. BCS-like density of states in superconducting $A_3C_{60}$ surfaces. *Phys. Rev. Lett.* **2000**, *85*, 1970−1973.
(37) Holczer, K.; Klein, O.; Huang, S.-M.; Kaner, R. B.; Fu, K.-J.; Whetten, R. L.; Diederich, F. Alkali-fulleride superconductors: Synthesis, composition, and diamagnetic shielding. *Science* **1991**, *252*, 1154−1157.
(38) Murphy, D. W.; Rosseinsky, M. J.; Fleming, R. M.; Tycko, R.; Ramirez, A. P.; Haddon, R. C.; Siegrist, T.; Dabbagh, G.; Tully, J. C.; Walstedt, R. E. Synthesis and characterization of alkali metal fullerides: $A_xC_{60}$. *J. Phys. Chem. Solids* **1992**, *53*, 1321−1332.
(39) Stepniak, F.; Benning, P. J.; Poirier, D. M.; Weaver, J. H. Electrical transport in Na, K, Rb, and Cs fullerides: Phase formation, microstructure, and metallicity. *Phys. Rev. B* **1993**, *48*, 1899−1906.
(40) Benning, P. J.; Stepniak, F.; Weaver, J. H. Electron-diffraction and photoelectron-spectroscopy studies of fullerene and alkali-metal fulleride films. *Phys. Rev. B* **1993**, *48*, 9086−9096.
(41) Yildirim, T.; Barbedette, L.; Fischer, J. E.; Lin, C. L.; Robert, J.; Petit, P.; Palstra, T. T. M. $T_c$ vs carrier concentration in cubic fulleride superconductors. *Phys. Rev. Lett.* **1996**, *77*, 167−170.
(42) Ren, M.-Q.; Han, S.; Wang, S.-Z.; Fan, J.-Q.; Song, C.-L.; Ma, X.-C.; Xue, Q.-K. Direct observation of full-gap superconductivity and pseudogap in two-dimensional fullerides. *Phys. Rev. Lett.* **2020**, *124*, 187001.
(43) Yoon, T.; Koo, J. Y.; Choi, H. C. High yield organic superconductors via solution-phase alkali metal doping at room temperature. *Nano Lett.* **2020**, *20*, 612−617.
(44) Zhou, P.; Wang, K.-A.; Rao, A. M.; Eklund, P. C.; Dresselhaus, G.; Dresselhaus, M. S. Raman-scattering studies of homogeneous $K_3C_{60}$ films. *Phys. Rev. B* **1992**, *45*, 10838−10840.
(45) Haddon, R. C.; Hebard, A. F.; Rosseinsky, M. J.; Murphy, D. W.; Duclos, S. J.; Lyons, K. B.; Miller, B.; Rosamilia, J. M.; Fleming, R. M.; Kortan, A. R.; et al. Conducting films of $C_{60}$ and $C_{70}$ by alkali-metal doping. *Nature* **1991**, *350*, 320−322.
(46) Kuzmany, H.; Pfeiffer, R.; Hulman, M.; Kramberger, C. Raman spectroscopy of fullerenes and fullerene-nanotube composites. *Philos. Trans. R. Soc. A Math. Phys. Eng. Sci.* **2004**, *362*, 2375−2406.
(47) Mitch, M. G.; Lannin, J. S. Raman scattering in $K_4C_{60}$ and $Rb_4C_{60}$ fullerenes. *Phys. Rev. B* **1995**, *51*, 6784−6787.
(48) Fleming, R. M.; Rosseinsky, M. J.; Ramirez, A. P.; Murphy, D. W.; Tully, J. C.; Haddon, R. C.; Siegrist, T.; Tycko, R.; Glarum, S. H.; Marsh, P.; et al. Preparation and structure of the alkali-metal fulleride $A_4C_{60}$. *Nature* **1991**, *352*, 701−703.
(49) Weaver, J. H.; Benning, P. J.; Stepniak, F.; Poirier, D. M. $K_xC_{60}$: Nonequilibrium thin film growth and spectroscopic results. *J. Phys. Chem. Solids* **1992**, *53*, 1707−1711.
(50) Bean, C. P. Magnetization of hard superconductors. *Phys. Rev. Lett.* **1962**, *8*, 250−253.
(51) Gömöry, F. Characterization of high-temperature superconductors by ac susceptibility measurements. *Supercond. Sci. Technol.* **1997**, *10*, 523−542.
(52) Palstra, T. T. M.; Haddon, R. C.; Hebard, A. F.; Zaanen, J. Electronic transport properties of $K_3C_{60}$ films. *Phys. Rev. Lett.* **1992**, *68*, 1054−1057.


https://doi.org/10.1021/acs.jpcc.1c10420
J. Phys. Chem. C 2022, 126, 2912−2919

(53) Holczer, K.; Klein, O.; Grüner, G.; Thompson, J. D.; Diederich, F.; Whetten, R. L. Critical magnetic fields in the superconducting state of $K_3C_{60}$. *Phys. Rev. Lett.* **1991**, *67*, 271−274.

(54) Irons, S. H.; Liu, J. Z.; Klavins, P.; Shelton, R. N. Magnetic properties of superconducting $K_3C_{60}$ and $Rb_3C_{60}$ synthesized from large single-crystal fullerenes. *Phys. Rev. B* **1995**, *52*, 15517−15521.

(55) Buntar, V.; Sauerzopf, F. M.; Weber, H. W. Lower critical fields of alkali-metal-doped fullerene superconductors. *Phys. Rev. B* **1996**, *54*, R9651−R9654.

(56) Werthamer, N. R.; Helfand, E.; Hohenberg, P. C. Temperature and Purity Dependence of the Superconducting Critical Field, $H_{c2}$. III. Electron spin and spin-orbit effects. *Phys. Rev.* **1966**, *147*, 295−302.

(57) Johnson, C. E.; Jiang, H. W.; Holczer, K.; Kaner, R. B.; Whetten, R. L.; Diederich, F. Upper-critical-field-temperature phase diagram of alkali-metal-intercalated $C_{60}$ superconductors. *Phys. Rev. B* **1992**, *46*, 5880−5882.

(58) Baenitz, M.; Straube, E.; Gärtner, S.; Werner, H.; Schlögl, R.; Lüders, K. Ac Susceptibility and upper critical fields in $Rb_3C_{60}$. *Fuller. Sci. Technol.* **1993**, *1*, 177−188.

(59) Foner, S.; McNiff, E. J., Jr.; Heiman, D.; Huang, S.-M.; Kaner, R. B. Measurements of the upper critical field of $K_3C_{60}$ and $Rb_3C_{60}$ powders to 60 T. *Phys. Rev. B* **1992**, *46*, 14936−14939.

(60) Kasahara, Y.; Takeuchi, Y.; Zadik, R. H.; Takabayashi, Y.; Colman, R. H.; McDonald, R. D.; Rosseinsky, M. J.; Prassides, K.; Iwasa, Y. Upper critical field reaches 90 T near the Mott transition in fulleride superconductors. *Nat. Commun.* **2017**, *8*, 14467.

(61) Tinkham, M. *Introduction to Superconductivity*, 1st ed.; McGraw-Hill: New York, 1996.

(62) Uemura, Y. J.; Keren, A.; Le, L. P.; Luke, G. M.; Wu, W. D.; Tsai, J. S.; Tanigaki, K.; Holczer, K.; Donovan, S.; Whetten, R. L. System dependence of the magnetic-field penetration depth in $C_{60}$ superconductors. *Physica C* **1994**, *235*, 2501−2502.

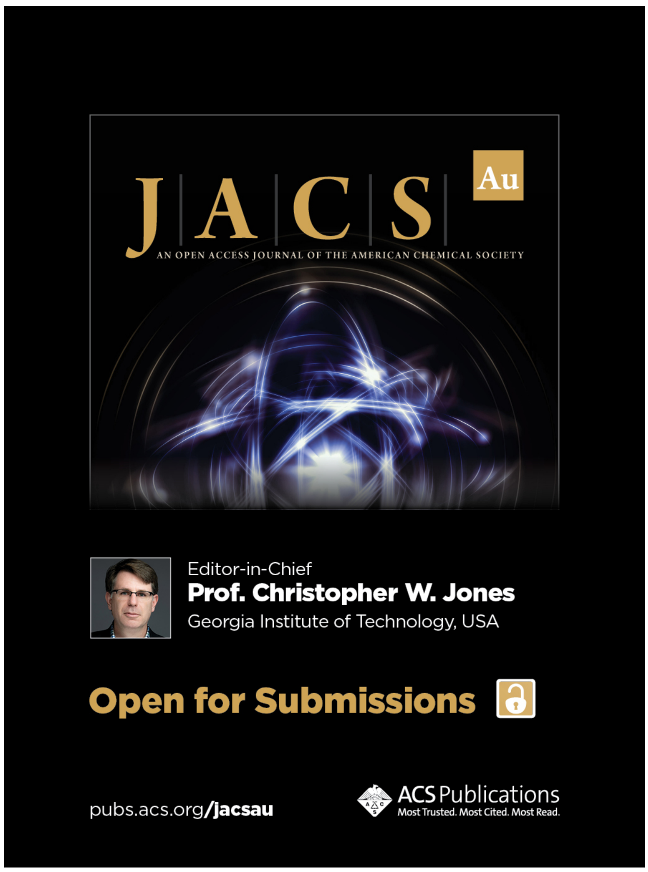




https://doi.org/10.1021/acs.jpcc.1c10420
J. Phys. Chem. C 2022, 126, 2912−2919